



Article

Theoretical Study on the Gas Phase and Gas–Liquid Interface Reaction Mechanism of Criegee Intermediates with Glycolic Acid Sulfate

Lei Li, Qingzhu Zhang *, Yuanyuan Wei, Qiao Wang and Wenxing Wang

Environment Research Institute, Shandong University, Qingdao 266237, China

* Correspondence: zqz@sdu.edu.cn

Abstract: Criegee intermediates (CIs) are important zwitterionic oxidants in the atmosphere, which affect the budget of OH radicals, amines, alcohols, organic/inorganic acids, etc. In this study, quantum chemical calculation and Born–Oppenheimer molecular dynamic (BOMD) simulation were performed to show the reaction mechanisms of C2 CIs with glycolic acid sulfate (GAS) at the gas-phase and gas–liquid interface, respectively. The results indicate that CIs can react with COOH and OSO₃H groups of GAS and generate hydroperoxide products. Intramolecular proton transfer reactions occurred in the simulations. Moreover, GAS acts as a proton donor and participates in the hydration of CIs, during which the intramolecular proton transfer also occurs. As GAS widely exists in atmospheric particulate matter, the reaction with GAS is one of the sink pathways of CIs in areas polluted by particulate matter.

Keywords: Criegee intermediates; glycolic acid sulfate; gas-phase reaction; aqueous-surface reaction; proton transfer



Citation: Li, L.; Zhang, Q.; Wei, Y.; Wang, Q.; Wang, W. Theoretical Study on the Gas Phase and Gas–Liquid Interface Reaction Mechanism of Criegee Intermediates with Glycolic Acid Sulfate. *Int. J. Mol. Sci.* **2023**, *24*, 3355. <https://doi.org/10.3390/ijms24043355>

Academic Editors: Andrei L. Tchougréeff, Rubicelia Vargas and Jorge Garza

Received: 20 December 2022

Revised: 9 January 2023

Accepted: 11 January 2023

Published: 8 February 2023



Copyright: © 2023 by the authors. Licensee MDPI, Basel, Switzerland. This article is an open access article distributed under the terms and conditions of the Creative Commons Attribution (CC BY) license (<https://creativecommons.org/licenses/by/4.0/>).

1. Introduction

The reactions of ozone with unsaturated hydrocarbons are important sources of free radicals and particulate matter in the atmosphere [1]. Criegee intermediates (CIs) are tropospheric biradical/zwitterionic species that are derived from the ozonolysis of alkenes [2]. Ozone undergoes 1,3-cycloaddition with a double bond of alkene to form a primary ozonide that subsequently decomposes into a carbonyl oxide (also called Criegee intermediate) and a carbonyl compound [3]. The energized Criegee intermediate, which is produced by exothermic decomposition and contains vibrational excitation, undergoes unimolecular decay or forms a stable Criegee intermediate via collisional quenching [4]. In addition to the above reaction, the contribution that formed through other reactions to the total CIs is inappreciable. The reaction of CH₃O₂ with OH radicals, affecting the concentrations of HO₂ and O₃ in the oceanic boundary layer, has been determined to produce trace amounts of CH₂OO (yield of CH₂OO < 5%) [5]. The oxidation of dimethyl sulfoxide forms CH₂OO at low temperatures, but the yield is too low to be a pivotal source of CIs [6].

The unimolecular decomposition of CIs, which occurs via the vinyl hydroperoxide pathway or the ester pathway, plays a significant role in the production of atmospheric OH radicals [7,8]. Elshorbany et al. [9] reported that the decomposition of CIs has a 24% contribution to the daytime OH radical formation. In addition, CI decomposition is a steady and dominant source of OH radicals at nighttime [10]. The PUMA campaign (a project that measured pollution of the urban midlands atmosphere in the UK) showed that ozonolysis of alkenes dominates the OH production in winter and accounts for more than 50% of the production in summer [11].

Even if most CIs decay through unimolecular pathways, a fraction of CIs survives for long enough to react with other substances. The reaction with water vapor is the

most efficient scavenging route for CIs in the troposphere [12]. Part of CIs react with water molecules and form low vapor pressure substances that act as cloud condensation nuclei (CCN) [13]. CH₂OO reacts with NO₂ to enhance NO₃ production in the urban atmosphere [14]. Dimethyl-substituted Criegee intermediate (CH₃)₂COO survives at high humidity to react with atmospheric SO₂, and the reaction rate ($1.3 \times 10^{-10} \text{ cm}^3\text{s}^{-1}$) is close to the gas kinetic limit [15]. The reactions of CIs with atmospheric organic matter play a significant role in the formation of secondary organic aerosol (SOA). The product of the CH₂OO + acrolein reaction is the secondary ozonide that has the potential to form SOA because of its large molecular weight [16]. Experimental and theoretical studies show that the reaction of CIs with alcohols represents a considerable source of α -alkoxyalkyl hydroperoxides (AAAHs) that form SOA with a production rate of 24 Gg year⁻¹ in tropical forests [17]. Despite the fact that the reactions of CIs with organics have been internationally recognized, the understanding of a Criegee–organosulfate reaction in the atmosphere is still developing.

Organosulfates (OSs), also known as sulfate esters or sulfate derivatives, are important organosulfur compounds that contain -OSO₃H group in the atmosphere [18,19]. Due to hydrophobic (the hydrocarbon group) and hydrophilic (the sulfate group) parts, OSs lower the surface tension of atmospheric particles, eventually changing the ability of particles to uptake water and to form CCN [20,21]. As OSs absorb sunlight, they significantly change the optical properties of organic aerosols and affect the energy balance of the atmosphere [22]. OSs react with oxidants such as OH, O₃, and NO_x in the atmospheric lifetime, which promotes the formation of SOA [23]. Accordingly, OSs have the potential to react with CIs. In the atmosphere, glycolic acid sulfate (GAS) is a common organosulfate with a -OSO₃H group and a -COOH group [24]. Some studies have reported the formation of aqueous-phase and heterogeneous OSs [25,26]. Most of the GAS is present in the ambient aerosols in the atmosphere [27]. Detection of OSs in summer in Beijing revealed that GAS is the most abundant among all quantified species, the concentrations of GAS in the thirteen OSs measured ambient aerosols ranged from 3.9 to 58.2 ng/m³ and the average concentration was 19.5 ng/m³ [28]. Olson et al. measured concentrations of OSs in particulate matter in the United States, Pakistan, and Mexico, where GAS concentrations ranged from 1.9–11.3 ng/m³ [29]. Therefore, it is necessary to investigate the reaction mechanism of CIs with GAS in the atmosphere.

This work explored the reaction mechanism of C2 CIs (*anti*- and *syn*-CH₃CHOO) with GAS using density functional theory (DFT). Due to the hydrophobic methyl group, C2 CIs have a longer lifetime at the gas–liquid interface compared to C1 CIs [30]. Therefore, the Born–Oppenheimer molecular dynamics (BOMD) was carried out to simulate the heterogeneous reactions of CH₃CHOO with GAS on the droplet surface. For the gas–liquid interface reactions, we consider the collision of GAS molecules in the atmosphere with CIs on the droplet rather than the collision reaction of CIs with GAS that is dissolved in the droplet.

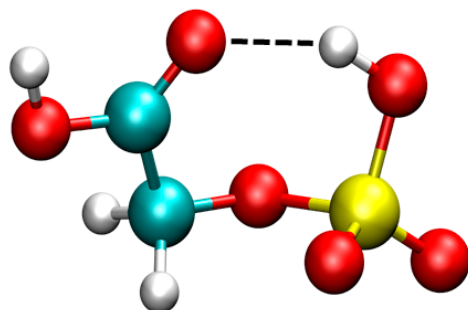
2. Results and Discussion

The most stable configuration of GAS is shown in Figure 1. A seven-membered ring structure is formed in the molecule. The hydrogen bond interaction was observed between the terminal hydrogen of the OSO₃H group and the carbonyl oxygen of the COOH group.

2.1. Gas-Phase Reactions

The values of relative Gibbs free energy (CCSD/6-311++G(2d,2p)) of the reactions between CH₃CHOO and GAS are displayed in Figure 2. The configurations of reaction complexes, transition states, and products are depicted in Figure S1. The reaction energy barriers of *syn*-CH₃CHOO with OSO₃H and COOH groups are 1.00 and 2.87 kcal/mol, respectively. The reactions of *anti*-CH₃CHOO with OSO₃H and COOH groups need to cross energy barriers of 3.30 and 4.09 kcal/mol, respectively. The low energy barriers suggest that these reactions are feasible in the atmosphere. Previous studies have shown that most

reactions of CIs with carboxylic acids follow a barrierless pathway [31,32]. However, we observed that the reactions of the COOH group with CH₃CHOO require overcoming the energy barrier, which may be due to the formation of a six-membered ring that increases the stability of GAS.



Glycolic acid sulfate (GAS)

Figure 1. The most stable configuration of GAS.

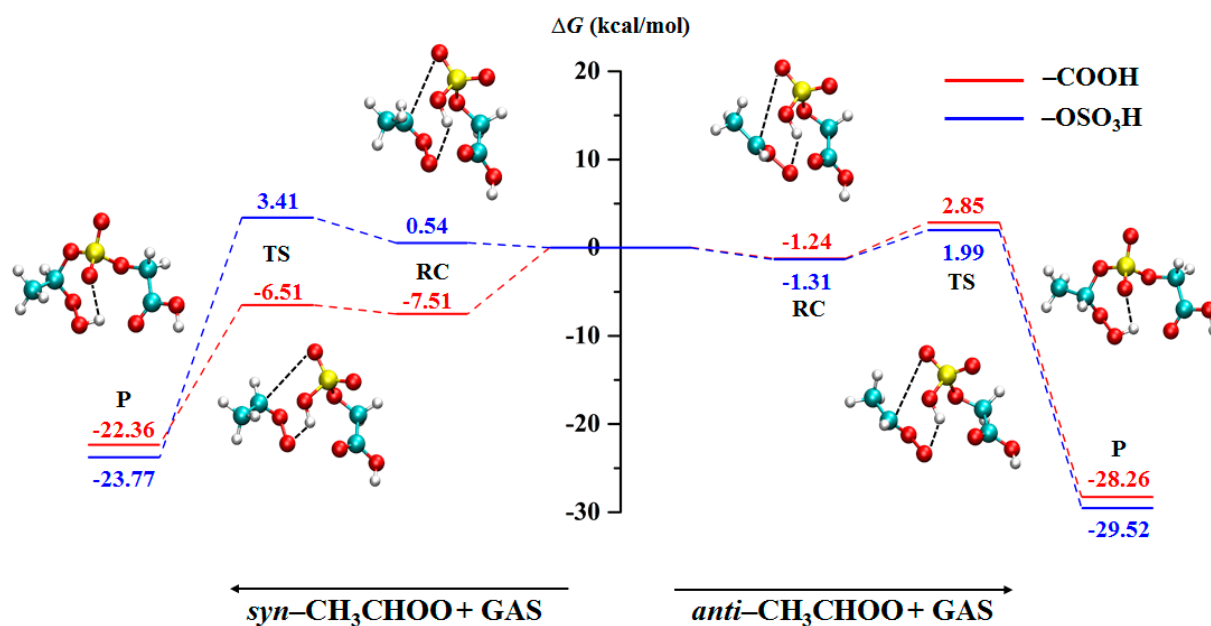


Figure 2. The minimum energy pathway of the direct reactions between CH₃CHOO and GAS.

Water molecules are one of the most abundant species in the atmosphere and have a significant impact on atmospheric chemical processes [33]. Therefore, the relative Gibbs free energy (CCSD/6-311++G(2d,2p)) of the water-mediated reactions between CH₃CHOO and GAS was calculated (Figure 3). The two lowest energy barriers are 0.78 and 2.55 kcal/mol, which are determined for the water-mediated reaction of *syn*-CH₃CHOO with the OSO₃H group and the reaction of *syn*-CH₃CHOO with the COOH group, respectively. Compared with the direct reactions of *syn*-CH₃CHOO, the water molecule lowers the energy barrier of the reaction with the OSO₃H group but increases the energy barrier of the reaction with the COOH group. In contrast, the water-mediated reaction barrier of *anti*-CH₃CHOO with OSO₃H group is increased to 6.11 kcal/mol, and that of *anti*-CH₃CHOO with COOH group is decreased to 3.43 kcal/mol. The participation of water molecules leads to the change of the reaction energy barrier to be less than 3 kcal/mol, indicating that the effect of water molecules on the reaction of CH₃CHOO with GAS is weak. The configurations of the water-mediated reaction stages are presented in Figure S2.

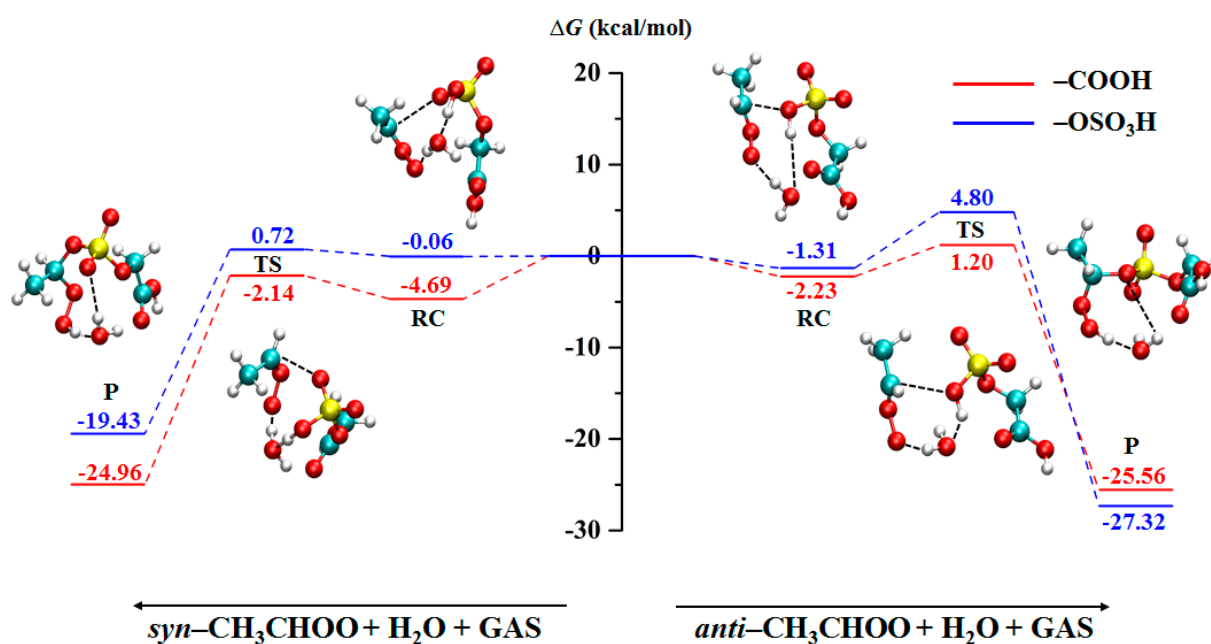


Figure 3. The minimum energy pathway of the water-mediated reactions between CH_3CHOO and GAS.

2.2. Gas–Liquid Interface Reactions

The gas–liquid interface plays a pivotal and ubiquitous role in atmospheric chemistry, including absorbing various pollutants and changing chemical reaction mechanisms. For example, Shang et al. [34] reported the interfacial reaction of SO_2 with oleic acid, which is a new pathway to form organosulfur in the atmosphere. In this study, the gas–liquid interface reaction mechanism of *anti*- CH_3CHOO with GAS was explored at the molecular level. In order to eliminate the effect of reaction location, thirty simulations were performed at different locations of the droplet. The reactions of *anti*- CH_3CHOO with GAS occurred in 16 simulations. The direct and water-mediated reactions of *anti*- CH_3CHOO with the COOH group occurred six and two times, respectively. The direct and water-mediated reactions of *anti*- CH_3CHOO with the OSO_3H group both occurred four times. The hydration reactions of *anti*- CH_3CHOO occurred 11 times.

2.2.1. Reaction of Anti- CH_3CHOO with the COOH Group of GAS

Figure 4a shows the structure and bond length variations of the direct reaction between *anti*- CH_3CHOO and the COOH group of GAS. Based on the properties of hydrophobicity and hydrophilicity, the methyl group of *anti*- CH_3CHOO is placed on the side away from the droplet. At 0 ps, the distances of H-O3, C-O1, and H-O2 are 0.97, 2.66, and 2.52 Å, respectively. Subsequently, the H atom of the COOH group gradually approaches the terminal oxygen of *anti*- CH_3CHOO , and the carbonyl oxygen of the COOH group approaches the α -carbon atom of *anti*- CH_3CHOO . At 0.14 ps, the distances of H-O3, C-O1, and H-O2 are 1.53, 2.13, and 1.00 Å, respectively, where the transition-state-like structure is formed. At 0.20 ps, the H atom on the COOH group binds to the terminal oxygen of *anti*- CH_3CHOO , and the C-O1 and H-O2 bonds are formed and remain stable, indicating the formation of the reaction product.

The mechanism of the water-mediated reaction between the *anti*- CH_3CHOO and COOH group of GAS (Figure 4b) is different from that of the direct reaction. At 0 ps, the initial distances of H2-O3, H1-O3, H2-O2, H1-O4, and C-O1 are 0.98, 2.40, 2.05, 0.97, and 3.22 Å, respectively. At 0.12 ps, the structure of the reactants is similar to the transition state; the distances of H2-O3, H1-O3, H2-O2, H1-O4, and C-O1 are 1.05, 1.22, 1.48, 1.24, and 2.66 Å, respectively. At 0.24 ps, H2-O2 and H1-O4 bonds are formed. However, the C-O1 bond (1.56 Å) is formed at 0.57 ps. In water-mediated reactions, the C-O1 bond is formed later than other bonds, and the water molecule is the bridge of proton transfer.

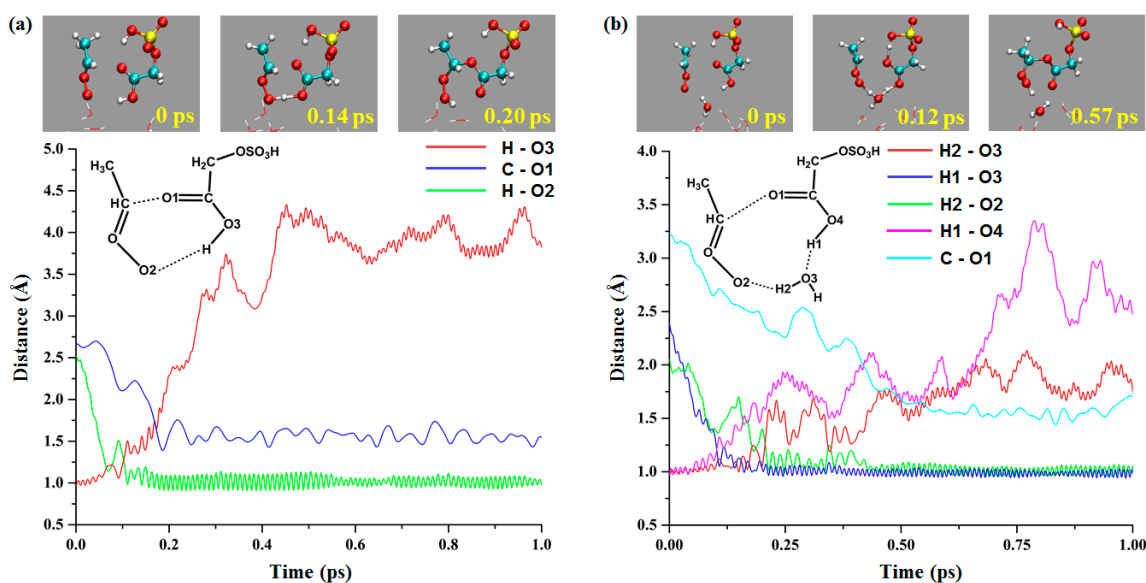


Figure 4. The direct and water-mediated reactions between *anti*-CH₃CHOO and COOH group of GAS at gas–liquid interface ((a): direct reaction; (b): water-mediated reaction).

2.2.2. Reaction of Anti-CH₃CHOO with the OSO₃H Group of GAS

The direct and water-mediated reactions between the *anti*-CH₃CHOO and OSO₃H groups of GAS were observed in our simulations (Figure 5). For the direct reaction, the distances of H-O2, H-O3, and C-O1 are 0.98, 2.48, and 4.04 Å, respectively, at 0 ps. From 0.38 to 0.63 ps, the H atom of the OSO₃H group vibrates between O3 and O2 atoms. The length of H-O3 fluctuates around 0.98 Å from 0.63 ps, but the distance of C-O1 is still decreasing. At 0.71 ps, the O1 atom of GAS binds to the C atom of *anti*-CH₃CHOO, indicating the formation of a hydroperoxide product.

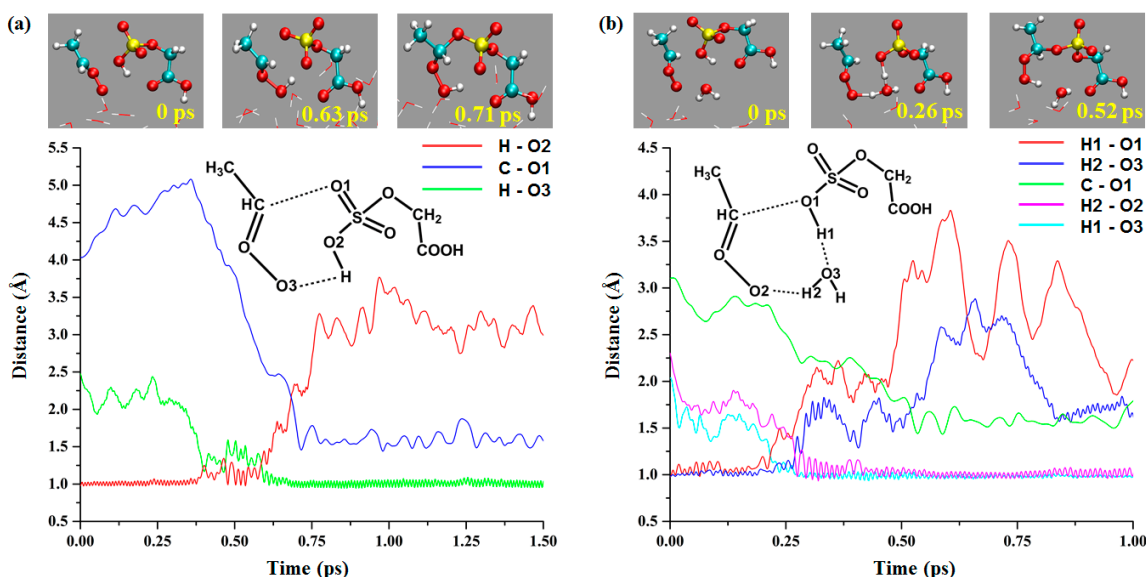


Figure 5. The direct and water-mediated reactions between *anti*-CH₃CHOO and OSO₃H group of GAS at gas–liquid interface ((a): direct reaction; (b): water-mediated reaction).

For the water-mediated reaction (Figure 5b), the initial distances of H2-O2, H1-O3, and C-O1 are 2.30, 2.03, and 3.10 Å, respectively. The transition-state-like structure is observed at 0.26 ps, where the lengths of H2-O2, H1-O3, H1-O1, H2-O3, and C-O1 are 1.41, 1.09, 1.39, 1.10, and 2.43 Å, respectively. The H2-O2 and H1-O3 are formed at 0.30

and 0.27 ps, respectively. The O1 atom binds to the C atom at 0.52 ps, which occurs later than the formation of the H2-O2 bond. This phenomenon is also observed in the water-mediated reaction between the COOH group of *anti*-CH₃CHOO and GAS, suggesting that water-mediated proton transfer initiates the reactions and promotes the binding of C and O atoms.

2.2.3. Intramolecular Proton Transfer Reaction of Anti-CH₃CHOO with the OSO₃H Group of GAS

Most of the previous studies have focused on the reaction of CIs with monofunctional species [35–37]. Even the study of CIs and multifunctional species is the independent reaction of a single functional group [38]. However, the reaction involving both functional groups of GAS is observed in this study (Figure 6). At 0 ps, the two interface water molecules are far away from *anti*-CH₃CHOO and GAS, and the distances of H2-O4 and H3-O2 are 3.68 and 3.92 Å, respectively. The transition-state-like complex of *anti*-CH₃CHOO, GAS, and water molecules is formed at 2.09 ps. The proton of the OSO₃H group is transferred to the carbonyl oxygen of the COOH group at this time; the distances of H1-O1 and H1-O6 are 1.15 and 1.44 Å, respectively. The proton of the COOH group moves to the water molecule, and the distances of H2-O5 and H2-O4 are 1.26 and 1.28 Å, respectively. In this way, proton transfer occurs between the two functional groups of GAS, and the COOH group acts as the shuttle of proton transfer in this reaction. At 2.37 ps, the H3-O2 bond (the length is 0.99 Å) is formed, indicating proton transfer between the four reactant molecules is complete. The C-O1 bond is formed at 2.79 ps, resulting in the formation of new products. During the whole reaction process, both the COOH group of GAS and water molecules act as bridges of proton transfer.

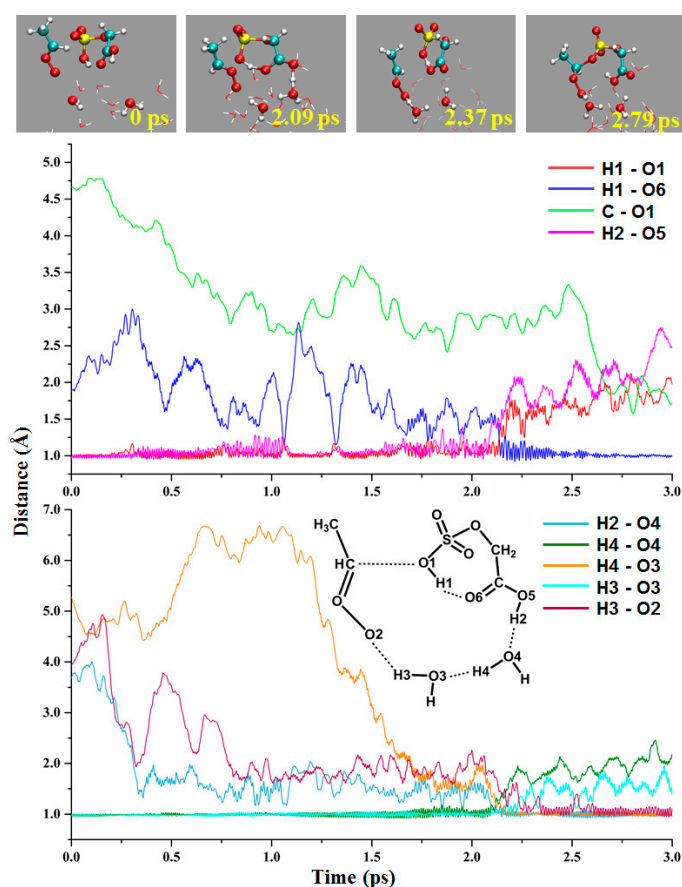


Figure 6. The intramolecular proton transfer reaction between *anti*-CH₃CHOO and OSO₃H group of GAS at gas–liquid interface.

2.2.4. GAS-Mediated Hydration of Anti-CH₃CHOO

Kumar et al. [39] reported BOMD simulations of *anti*-CH₃CHOO reacting with HNO₃ at the gas–liquid interface, suggesting that HNO₃-mediated *anti*-CH₃CHOO hydration is the most dominant reaction. In this study, the GAS-mediated hydration of *anti*-CH₃CHOO occurs and generates C₂H₃O₆[−] and H₃O⁺ ions, and the reaction follows an obvious stepwise mechanism. As shown in Figure 7, *anti*-CH₃CHOO and GAS are placed on the droplet surface, which is far from the water molecules at 0 ps. For the first step, the proton on the COOH group is transferred to the terminal oxygen of *anti*-CH₃CHOO, and the intramolecular proton transfer occurs in GAS. At 1.86 ps, the distances of H1-O1 and H5-O7 are 1.18 and 1.24 Å, respectively. At 2.10 ps, the distances of H1-O1 and H5-O7 are 0.98 and 1.01 Å, respectively, indicating the protonated *anti*-CH₃CHOO and C₂H₃O₆[−] ion are formed. In the second step, the O atom of the water molecule combines with α-C of the *anti*-CH₃CHOO, and the proton is transferred to another water molecule. At 2.52 ps, the distances of C-O2 and H2-O3 are 1.41 and 0.98 Å, respectively. In this last step, the water molecules transfer protons to each other, and the H₃O⁺ ion is formed at 4.85 ps. In this pathway, GAS acts as a water molecule to provide protons for the hydration of *anti*-CH₃CHOO.

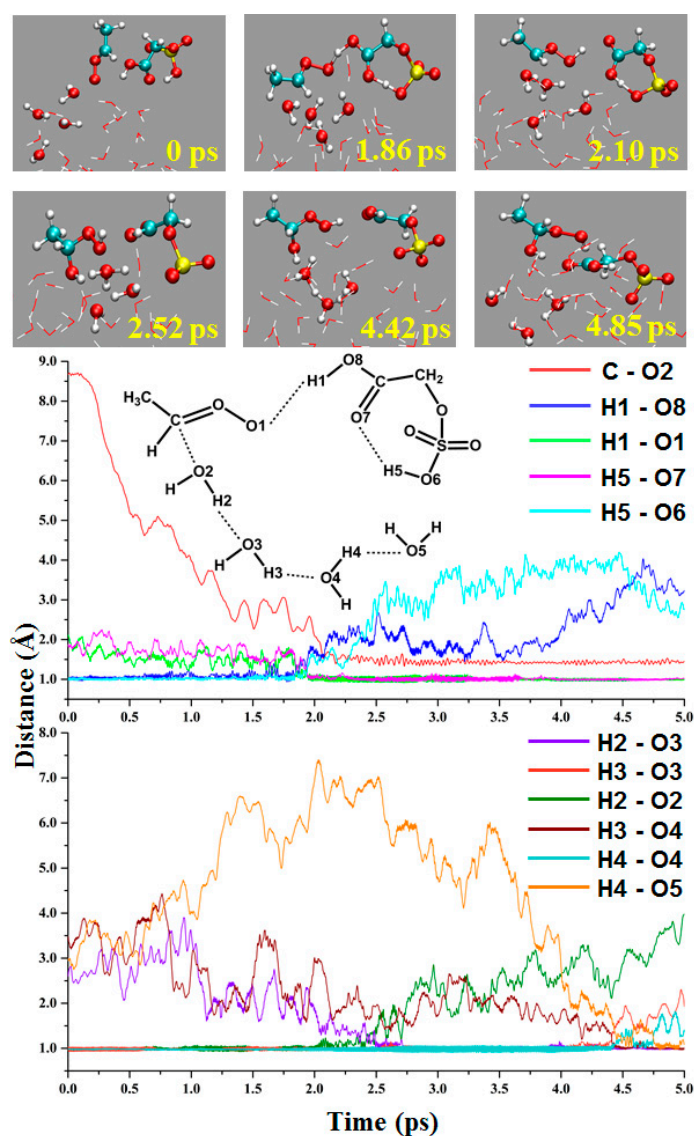


Figure 7. The GAS-mediated hydration of *anti*-CH₃CHOO at gas–liquid interface.

3. Atmospheric Implications

These results deepen the understanding of CI fate in the atmosphere. GAS is an abundant nucleation precursor and has an important contribution to the formation of atmospheric particulate pollution [40–42]. The reaction with GAS is one of the sink pathways for CH_3CHOO , especially the direct reaction with the COOH group is a nearly barrierless process (1.00 kcal/mol), which may be the dominant reaction in a dry atmosphere. The water-mediated reaction between CH_3CHOO and OSO_3H groups is also a nearly barrierless process (0.78 kcal/mol), which may be the dominant reaction in polluted areas with high humidity.

Furthermore, the BOMD simulations reveal the reaction mechanism of *anti*- CH_3CHOO with GAS on droplets. Both direct and water-mediated reactions are observed, with the formation of ring structures during the reaction. Among them, the water-mediated reaction follows the proton transfer mechanism, and the water molecule acts as a bridge for proton transfer. Although it has been reported that CH_3CHOO can exist stably on the droplet surface [30], all the reactions of *anti*- CH_3CHOO with GAS on the droplet occur on the ps timescale. The terminal O atom of *anti*- CH_3CHOO binding to the H atom of GAS in the reaction occurs slightly later than the α -C atom of *anti*- CH_3CHOO binding to the O atom of GAS, suggesting the reactions are initiated by the binding of O and H atoms. Both quantum chemical calculations and molecular simulations indicate that water molecules can participate in the reaction of CH_3CHOO with GAS. In addition, though the reaction of CIs with various species on droplets is discussed in the literature [43–46], intramolecular proton transfer was observed in our simulations. The hydrogen bond and six-membered ring structure are formed inside the GAS molecule, resulting in the intramolecular proton transfer. It is believed that similar reactions can occur in some substances with longer carbon chains and multiple functional groups in the atmosphere. GAS-promoted hydration of *anti*- CH_3CHOO as a proton donor was also observed in the simulations. Previous studies have pointed out that nitric acid and methanesulfonic acid promote CIs hydration [39,47]; GAS also tends to perform intramolecular proton transfer while donating a proton, which has appeared many times in the simulations.

The product of CH_3CHOO reacting with GAS is hydroperoxides. Hydroperoxides participate in the formation of new particles, and SOA in the atmosphere [48–50], which have toxic effects on human health and plants [51–53], and some macromolecular hydroperoxides can act as CCN [39]. The reactions of CH_3CHOO with GAS increase the carbon chain length and the ability to form hydrogen bonds, which has great potential in particle formation.

4. Materials and Methods

The 72 configurations of GAS were optimized, and the most stable configuration was selected as the reactant. The configuration optimization and transition state searching were conducted with the M06-2X method [54] in conjunction with the 6-311++G(2d,2p) basis set. The analysis of intrinsic reaction coordinates (IRC) [55,56] was used to verify that all transition states connect to the expected reactants and products. Single point energies of reactants, complexes, transition states, and products were calculated at the CCSD/6-311++G(2d,2p) level. All calculations of electronic structures were performed with Gaussian 09 program [57].

Thirty gas–liquid interface simulations were carried out by BOMD. All simulations were performed by CP2K [58] software based on the DFT method. The droplet consisted of 30 water molecules, and reactants were placed in a cubic box with the side length set as 35 Å. The Becke–Lee–Yang–Parr (BLYP) [59,60] functional, double- ζ Gaussian basis set (DZVP) [61] and Goedecker–Teter–Hutter (GTH) norm-conserved pseudopotentials [62,63] were adopted to handle electronic exchange interaction, valence and core electrons, respectively. All BOMD simulations were performed in the constant volume and temperature (NVT) ensemble with the integration step of 1 fs. The system temperature (300 K) was controlled using the Nose-Hoover chain method.

Supplementary Materials: The following supporting information can be downloaded at: <https://www.mdpi.com/article/10.3390/ijms24043355/s1>.

Author Contributions: Conceptualization, L.L., Y.W. and Q.W.; Data curation, L.L., Y.W. and Q.W.; Formal analysis, L.L.; Funding acquisition, Q.Z.; Methodology, L.L.; Supervision, W.W.; Writing—original draft, L.L. and Y.W.; Writing—review and editing, Q.Z. All authors have read and agreed to the published version of the manuscript.

Funding: This work was supported by NSFC (National Natural Science Foundation of China, project Nos. 22236004, 21976107, 42075106, 42175122).

Data Availability Statement: The configurations of the direct and water-mediated reaction stages (reaction complex, transition state and product).

Conflicts of Interest: The authors declare that they have no known competing financial interests or personal relationships that could have appeared to influence the work reported in this paper.

References

1. Johnson, D.; Marston, G. The gas-phase ozonolysis of unsaturated volatile organic compounds in the troposphere. *Chem. Soc. Rev.* **2008**, *37*, 699–716. [[CrossRef](#)] [[PubMed](#)]
2. Criegee, R. Mechanism of Ozonolysis. *Angew. Chem. Int. Ed.* **1975**, *14*, 745–752. [[CrossRef](#)]
3. Taatjes, C.A.; Shallcross, D.E.; Percival, C.J. Research frontiers in the chemistry of Criegee intermediates and tropospheric ozonolysis. *Phys. Chem. Chem. Phys.* **2014**, *16*, 1704–1718. [[CrossRef](#)]
4. Horie, O.; Moortgat, G.K. Gas-Phase Ozonolysis of Alkenes. Recent Advances in Mechanistic Investigations. *Acc. Chem. Res.* **1998**, *31*, 387–396. [[CrossRef](#)]
5. Assaf, E.; Sheps, L.; Whalley, L.; Heard, D.; Tomas, A.; Schoemaeker, C.; Fittschen, C. The Reaction between CH₃O₂ and OH Radicals: Product Yields and Atmospheric Implications. *Environ. Sci. Technol.* **2017**, *51*, 2170–2177. [[CrossRef](#)]
6. Asatryan, R.; Bozzelli, J.W. Formation of a Criegee intermediate in the low-temperature oxidation of dimethyl sulfoxide. *Phys. Chem. Chem. Phys.* **2008**, *10*, 1769–1780. [[CrossRef](#)]
7. Lester, M.I.; Klippenstein, S.J. Unimolecular Decay of Criegee Intermediates to OH Radical Products: Prompt and Thermal Decay Processes. *Acc. Chem. Res.* **2018**, *51*, 978–985. [[CrossRef](#)]
8. Novelli, A.; Vereecken, L.; Lelieveld, J.; Harder, H. Direct observation of OH formation from stabilised Criegee intermediates. *Phys. Chem. Phys.* **2014**, *16*, 19941–19951. [[CrossRef](#)]
9. Elshorbany, Y.; Barnes, I.; Becker, K.H.; Kleffmann, J.; Wiesen, P. Sources and Cycling of Tropospheric Hydroxyl Radicals—An Overview. *Z. Phys. Chem.* **2010**, *224*, 967–987. [[CrossRef](#)]
10. Stone, D.; Whalley, L.K.; Heard, D.E. Tropospheric OH and HO₂ radicals: Field measurements and model comparisons. *Chem. Soc. Rev.* **2012**, *41*, 6348–6404. [[CrossRef](#)]
11. Harrison, R.; Yin, J.; Tilling, R.; Cai, X.; Seakins, P.; Hopkins, J.; Lansley, D.; Lewis, A.; Hunter, M.; Heard, D.; et al. Measurement and modelling of air pollution and atmospheric chemistry in the U.K. West Midlands conurbation: Overview of the PUMA Consortium project. *Sci. Total Environ.* **2006**, *360*, 5–25. [[CrossRef](#)]
12. Khan, M.A.H.; Percival, C.J.; Caravan, R.L.; Taatjes, C.A.; Shallcross, D.E. Criegee intermediates and their impacts on the troposphere. *Environ. Sci. Process. Impacts* **2018**, *20*, 437–453. [[CrossRef](#)] [[PubMed](#)]
13. Docherty, K.S.; Ziemann, P.J. Effects of Stabilized Criegee Intermediate and OH Radical Scavengers on Aerosol Formation from Reactions of β-Pinene with O₃. *Aerosol Sci. Technol.* **2003**, *37*, 877–891. [[CrossRef](#)]
14. Ouyang, B.; McLeod, M.W.; Jones, R.L.; Bloss, W.J. NO₃ radical production from the reaction between the Criegee intermediate CH₂OO and NO₂. *Phys. Chem. Chem. Phys.* **2013**, *15*, 17070–17075. [[CrossRef](#)]
15. Huang, H.-L.; Chao, W.; Lin, J.J.-M. Kinetics of a Criegee intermediate that would survive high humidity and may oxidize atmospheric SO₂. *Proc. Natl. Acad. Sci. USA* **2015**, *112*, 10857–10862. [[CrossRef](#)]
16. Zhou, X.; Chen, Y.; Liu, Y.; Li, X.; Dong, W.; Yang, X. Kinetics of CH₂OO and Syn-CH₃CHOO Reaction with Acrolein. *Phys. Chem. Chem. Phys.* **2021**, *23*, 13276–13283. [[CrossRef](#)]
17. McGillen, M.R.; Curchod, B.F.; Chhantyal-Pun, R.; Beames, J.M.; Watson, N.P.; Khan, M.A.H.; McMahon, L.; Shallcross, D.E.; Orr-Ewing, A.J. Criegee Intermediate–Alcohol Reactions, A Potential Source of Functionalized Hydroperoxides in the Atmosphere. *ACS Earth Space Chem.* **2017**, *1*, 664–672. [[CrossRef](#)]
18. Reemtsma, T.; These, A.; Venkatachari, P.; Xia, X.; Hopke, P.K.; Springer, A.; Linscheid, M. Identification of Fulvic Acids and Sulfated and Nitrated Analogues in Atmospheric Aerosol by Electrospray Ionization Fourier Transform Ion Cyclotron Resonance Mass Spectrometry. *Anal. Chem.* **2006**, *78*, 8299–8304. [[CrossRef](#)]
19. Surratt, J.D.; Kroll, J.H.; Kleindienst, T.E.; Edney, E.O.; Claeys, M.; Sorooshian, A.; Ng, N.L.; Offenberg, J.H.; Lewandowski, M.; Jaoui, M.; et al. Evidence for Organosulfates in Secondary Organic Aerosol. *Environ. Sci. Technol.* **2007**, *41*, 517–527. [[CrossRef](#)] [[PubMed](#)]

20. Hansen, A.M.K.; Hong, J.; Raatikainen, T.; Kristensen, K.; Ylisirniö, A.; Virtanen, A.; Petäjä, T.; Glasius, M.; Prisle, N.L. Hygroscopic properties and cloud condensation nuclei activation of limonene-derived organosulfates and their mixtures with ammonium sulfate. *Atmos. Meas. Tech.* **2015**, *15*, 14071–14089. [[CrossRef](#)]
21. Nozière, B.; Ekström, S.; Alsberg, T.; Holmström, S. Radical-initiated Formation of Organosulfates and Surfactants in Atmospheric Aerosols. *Geophys. Res. Lett.* **2010**, *37*, L05806. [[CrossRef](#)]
22. Fleming, L.T.; Ali, N.N.; Blair, S.L.; Roveretto, M.; George, C.; Nizkorodov, S.A. Formation of Light-Absorbing Organosulfates during Evaporation of Secondary Organic Material Extracts in the Presence of Sulfuric Acid. *ACS Earth Space Chem.* **2019**, *3*, 947–957. [[CrossRef](#)]
23. Romero, F.; Oehme, M. Organosulfates—A New Component of Humic-Like Substances in Atmospheric Aerosols? *J. Atmos. Chem.* **2005**, *52*, 283–294. [[CrossRef](#)]
24. Surratt, J.D.; Gómez-González, Y.; Chan, A.W.H.; Vermeylen, R.; Shahgholi, M.; Kleindienst, T.E.; Edney, E.O.; Offenberg, J.H.; Lewandowski, M.; Jaoui, M.; et al. Organosulfate Formation in Biogenic Secondary Organic Aerosol. *J. Phys. Chem. A* **2008**, *112*, 8345–8378. [[CrossRef](#)]
25. McNeill, V.F. Aqueous Organic Chemistry in the Atmosphere: Sources and Chemical Processing of Organic Aerosols. *Environ. Sci. Technol.* **2015**, *49*, 1237–1244. [[CrossRef](#)]
26. McNeill, V.F.; Woo, J.L.; Kim, D.D.; Schwier, A.N.; Wannell, N.J.; Sumner, A.J.; Barakat, J.M. Aqueous-Phase Secondary Organic Aerosol and Organosulfate Formation in Atmospheric Aerosols: A Modeling Study. *Environ. Sci. Technol.* **2012**, *46*, 8075–8081. [[CrossRef](#)] [[PubMed](#)]
27. Brüggemann, M.; Xu, R.; Tilgner, A.; Kwong, K.C.; Mutzel, A.; Poon, H.Y.; Otto, T.; Schaefer, T.; Poulain, L.; Nin Chan, M.; et al. Organosulfates in Ambient Aerosol: State of Knowledge and Future Research Directions on Formation, Abundance, Fate, and Importance. *Environ. Sci. Technol.* **2020**, *54*, 3767–3782. [[CrossRef](#)]
28. Wang, Y.; Hu, M.; Guo, S.; Wang, Y.; Zheng, J.; Yang, Y.; Zhu, W.; Tang, R.; Li, X.; Liu, Y.; et al. The secondary formation of organosulfates under interactions between biogenic emissions and anthropogenic pollutants in summer in Beijing. *Atmos. Meas. Tech.* **2018**, *18*, 10693–10713. [[CrossRef](#)]
29. Olson, C.N.; Galloway, M.M.; Yu, G.; Hedman, C.J.; Lockett, M.R.; Yoon, T.; Stone, E.A.; Smith, L.M.; Keutsch, F.N. Hydroxycarboxylic Acid-Derived Organosulfates: Synthesis, Stability, and Quantification in Ambient Aerosol. *Environ. Sci. Technol.* **2011**, *45*, 6468–6474. [[CrossRef](#)] [[PubMed](#)]
30. Zhong, J.; Kumar, M.; Zhu, C.Q.; Francisco, J.S.; Zeng, X.C. Surprising Stability of Larger Criegee Intermediates on Aqueous Interfaces. *Angew. Chem. Int. Ed. Engl.* **2017**, *56*, 7740–7744. [[CrossRef](#)] [[PubMed](#)]
31. Chhantyal-Pun, R.; McGillen, M.R.; Beames, J.M.; Khan, M.A.H.; Percival, C.J.; Shallcross, D.E.; Orr-Ewing, A.J. Temperature-Dependence of the Rates of Reaction of Trifluoroacetic Acid with Criegee Intermediates. *Angew. Chem. Int. Ed.* **2017**, *56*, 9044–9047. [[CrossRef](#)] [[PubMed](#)]
32. Vereecken, L. The reaction of Criegee intermediates with acids and enols. *Phys. Chem. Chem. Phys.* **2017**, *19*, 28630–28640. [[CrossRef](#)] [[PubMed](#)]
33. Buszek, R.J.; Francisco, J.S.; Anglada, J.M. Water effects on atmospheric reactions. *Int. Rev. Phys. Chem.* **2011**, *30*, 335–369. [[CrossRef](#)]
34. Shang, J.; Passananti, M.; Dupart, Y.; Ciuraru, R.; Tinel, L.; Rossignol, S.; Perrier, S.; Zhu, T.; George, C. SO₂ Uptake on Oleic Acid: A New Formation Pathway of Organosulfur Compounds in the Atmosphere. *Environ. Sci. Technol. Lett.* **2016**, *3*, 67–72. [[CrossRef](#)]
35. Chhantyal-Pun, R.; Rotavera, B.; McGillen, M.R.; Khan, M.A.H.; Eskola, A.J.; Caravan, R.L.; Blacker, L.; Tew, D.P.; Osborn, D.L.; Percival, C.J.; et al. Criegee Intermediate Reactions with Carboxylic Acids: A Potential Source of Secondary Organic Aerosol in the Atmosphere. *ACS Earth Space Chem.* **2018**, *2*, 833–842. [[CrossRef](#)]
36. Cornwell, Z.A.; Harrison, A.W.; Murray, C. Kinetics of the Reactions of CH₂OO with Acetone, alpha-Diketones, and beta-Diketones. *J. Phys. Chem. A* **2021**, *125*, 8557–8571. [[CrossRef](#)] [[PubMed](#)]
37. Elsamra, R.M.I.; Jalan, A.; Buras, Z.J.; Middaugh, J.E.; Green, W.H. Temperature and Pressure-Dependent Kinetics of CH₂OO + CH₃COCH₃ and CH₂OO + CH₃CHO: Direct Measurements and Theoretical Analysis. *Int. J. Chem. Kinet.* **2016**, *48*, 474–488. [[CrossRef](#)]
38. Ma, X.; Zhao, X.; Wei, Y.; Wang, W.; Xu, F.; Zhang, Q.; Wang, W. Effect of multifunctional compound monoethanolamine on Criegee intermediates reactions and its atmospheric implications. *Sci. Total Environ.* **2020**, *715*, 136812. [[CrossRef](#)]
39. Kumar, M.; Zhong, J.; Zeng, X.C.; Francisco, J.S. Reaction of Criegee Intermediate with Nitric Acid at the Air–Water Interface. *J. Am. Chem. Soc.* **2018**, *140*, 4913–4921. [[CrossRef](#)]
40. Hettiyadura, A.P.S.; Al-Naiema, I.M.; Hughes, D.D.; Fang, T.; Stone, E.A. Organosulfates in Atlanta, Georgia: Anthropogenic influences on biogenic secondary organic aerosol formation. *Atmos. Meas. Tech.* **2019**, *19*, 3191–3206. [[CrossRef](#)]
41. Le Breton, M.; Wang, Y.; Hallquist, Å.M.; Pathak, R.K.; Zheng, J.; Yang, Y.; Shang, D.; Glasius, M.; Bannan, T.J.; Liu, Q.; et al. Online Gas- and Particle-phase Measurements of Organosulfates, Organosulfonates and Nitrooxy Organosulfates in Beijing Utilizing a FIGAERO ToF-CIMS. *Atmos. Chem. Phys.* **2018**, *18*, 10355–10371. [[CrossRef](#)]
42. Wang, Y.; Zhao, Y.; Wang, Y.; Yu, J.-Z.; Shao, J.; Liu, P.; Zhu, W.; Cheng, Z.; Li, Z.; Yan, N.; et al. Organosulfates in atmospheric aerosols in Shanghai, China: Seasonal and interannual variability, origin, and formation mechanisms. *Atmos. Meas. Tech.* **2021**, *21*, 2959–2980. [[CrossRef](#)]

43. Liu, J.; Liu, Y.; Yang, J.; Zeng, X.C.; He, X. Directional Proton Transfer in the Reaction of the Simplest Criegee Intermediate with Water Involving the Formation of Transient H_3O^+ . *J. Phys. Chem. Lett.* **2021**, *12*, 3379–3386. [[CrossRef](#)]
44. Qiu, J.; Ishizuka, S.; Tonokura, K.; Colussi, A.J.; Enami, S. Reactivity of Monoterpene Criegee Intermediates at Gas–Liquid Interfaces. *J. Phys. Chem. A* **2018**, *122*, 7910–7917. [[CrossRef](#)] [[PubMed](#)]
45. Zhang, T.; Wen, M.; Ding, C.; Zhang, Y.; Ma, X.; Wang, Z.; Lily, M.; Liu, J.; Wang, R. Multiple evaluations of atmospheric behavior between Criegee intermediates and HCHO: Gas-phase and air-water interface reaction. *J. Environ. Sci.* **2023**, *127*, 308–319. [[CrossRef](#)]
46. Zhu, C.; Kumar, M.; Zhong, J.; Li, L.; Francisco, J.S.; Zeng, X.C. New Mechanistic Pathways for Criegee–Water Chemistry at the Air/Water Interface. *J. Am. Chem. Soc.* **2016**, *138*, 11164–11169. [[CrossRef](#)] [[PubMed](#)]
47. Ma, X.; Zhao, X.; Huang, Z.; Wang, J.; Lv, G.; Xu, F.; Zhang, Q.; Wang, W. Determination of reactions between Criegee intermediates and methanesulfonic acid at the air-water interface. *Sci. Total Environ.* **2020**, *707*, 135804. [[CrossRef](#)]
48. Docherty, K.S.; Wu, W.; Bin Lim, Y.; Ziemann, P.J. Contributions of Organic Peroxides to Secondary Aerosol Formed from Reactions of Monoterpenes with O_3 . *Environ. Sci. Technol.* **2005**, *39*, 4049–4059. [[CrossRef](#)]
49. Ehn, M.; Thornton, J.A.; Kleist, E.; Sipilä, M.; Junninen, H.; Pullinen, I.; Springer, M.; Rubach, F.; Tillmann, R.; Lee, B.; et al. A large source of low-volatility secondary organic aerosol. *Nature* **2014**, *506*, 476–479. [[CrossRef](#)]
50. Li, H.; Chen, Z.; Huang, L.; Huang, D. Organic peroxides' gas-particle partitioning and rapid heterogeneous decomposition on secondary organic aerosol. *Atmos. Meas. Tech.* **2016**, *16*, 1837–1848. [[CrossRef](#)]
51. Marklund, S. Actions of Hydroxymethylhydroperoxide and Bis(Hydroxymethyl)Peroxide on Fumarate Hydratase, Lactate-Dehydrogenase, Aspartate Aminotransferase, Glucose Oxidase, and Acid-Phosphatase. *Biochim. Biophys. Acta Biomembr.* **1972**, *258*, 9–16. [[CrossRef](#)] [[PubMed](#)]
52. Marklund, S. Mechanisms of the irreversible inactivation of horseradish peroxidase caused by hydroxymethylhydroperoxide. *Arch. Biochem. Biophys.* **1973**, *154*, 614–622. [[CrossRef](#)]
53. Wang, Z.; Herbinet, O.; Hansen, N.; Battin-Leclerc, F. Exploring hydroperoxides in combustion: History, recent advances and perspectives. *Prog. Energy Combust. Sci.* **2019**, *73*, 132–181. [[CrossRef](#)]
54. Zhao, Y.; Truhlar, D.G. The M06 suite of density functionals for main group thermochemistry, thermochemical kinetics, noncovalent interactions, excited states, and transition elements: Two new functionals and systematic testing of four M06-class functionals and 12 other functionals. *Theor. Chem. Acc.* **2008**, *120*, 215–241. [[CrossRef](#)]
55. Fukui, K. The path of chemical reactions—The IRC approach. *Acc. Chem. Res.* **1981**, *14*, 363–368. [[CrossRef](#)]
56. Hratchian, H.P.; Schlegel, H.B. Accurate reaction paths using a Hessian based predictor–corrector integrator. *J. Chem. Phys.* **2004**, *120*, 9918–9924. [[CrossRef](#)]
57. Frisch, M.J.; Trucks, G.W.; Schlegel, H.B.; Scuseria, G.E.; Robb, M.A.; Cheeseman, J.R.; Scalmani, G.; Barone, V.; Petersson, G.A.; Nakatsuji, H.; et al. *Gaussian 09, Revision B.01*; Gaussian Inc.: Wallingford, CT, USA, 2010.
58. VandeVondele, J.; Krack, M.; Mohamed, F.; Parrinello, M.; Chassaing, T.; Hutter, J. Quickstep: Fast and accurate density functional calculations using a mixed Gaussian and plane waves approach. *Comput. Phys. Commun.* **2005**, *167*, 103–128. [[CrossRef](#)]
59. Becke, A.D. Density-functional exchange-energy approximation with correct asymptotic behavior. *Phys. Rev. A* **1988**, *38*, 3098–3100. [[CrossRef](#)]
60. Lee, C.; Yang, W.; Parr, R.G. Development of the Colle-Salvetti correlation-energy formula into a functional of the electron density. *Phys. Rev. B* **1988**, *37*, 785–789. [[CrossRef](#)]
61. VandeVondele, J.; Hutter, J. Gaussian basis sets for accurate calculations on molecular systems in gas and condensed phases. *J. Chem. Phys.* **2007**, *127*, 114105. [[CrossRef](#)]
62. Goedecker, S.; Teter, M.; Hutter, J. Separable dual-space Gaussian pseudopotentials. *Phys. Rev. B* **1996**, *54*, 1703–1710. [[CrossRef](#)] [[PubMed](#)]
63. Hartwigsen, C.; Goedecker, S.; Hutter, J. Relativistic separable dual-space Gaussian pseudopotentials from H to Rn. *Phys. Rev. B* **1998**, *58*, 3641–3662. [[CrossRef](#)]

Disclaimer/Publisher's Note: The statements, opinions and data contained in all publications are solely those of the individual author(s) and contributor(s) and not of MDPI and/or the editor(s). MDPI and/or the editor(s) disclaim responsibility for any injury to people or property resulting from any ideas, methods, instructions or products referred to in the content.